Electronic Supplementary Information

Functionalized polyoxometalates enable fast ion transport in solid-state batteries at room temperature

Fangcheng Liu[a], Shicheng Han[a], Liwei Dong[a,b] and Xikui Fang[a,*]

[a] MIIT Key Laboratory of Critical Materials Technology for New Energy Conversion and Storage, School of Chemistry and Chemical Engineering, Harbin Institute of Technology, Harbin 150001 (China)
[b] State Key Laboratory of Space Power-Sources, Shanghai Institute of Space Power-Sources, Shanghai 200245 (China)

[*]E-mail address: xkfang@hit.edu.cn

Table of Contents **Page**

(1) Materials and Syntheses

All reagents were from Alfa Aesar, Aladdin, Sigma-Aldrich, Acros, Adamas-beta and used without further purification. Deionized water was used for sample preparation.

1.1 Synthesis of $(DMA)_3H_3[Mn_3PW_9O_{34}(PDC)_3]\cdot 7H_2O$ ($(DMA)_3H_3$**1**$\cdot 7H_2O$)

The tri-vacant Keggin precursor $Na_9[A\text{-}\alpha\text{-}PW_9O_{34}]\cdot 7H_2O$({A-$\alpha$-$PW_9$}) was prepared according to the previous literature method.[1]

A sample of {A-α-PW_9} (0.256 g, 0.10 mmol) was suspended in 40 mL water, and (0.134 g, 0.50 mmol) manganese acetate dihydrate was added. The mixture was stirred for 3 min at room temperature until a brown red solution formed. Pyridine-2,6-dicarboxylic acid (H_2PDC) (0.1 g, 0.6 mmol) was added in the above solution. After heating at 80 ℃ for 1 h, dimethylamine hydrochloride (0.6 g, 7.36 mmol) was added to the above solution. The solution was filtered and dark brown prismatic crystals were harvested after approximately a week, yield 0.38 g, 72% based on Mn. Elemental analysis, calculated: H, 1.50; C, 10.28; Mn, 5.23; N, 2.66; P, 0.98; W, 52.48%. found: H, 1.42; C, 9.26; Mn, 6.24; N, 2.64; P, 1.19; W, 53.58%. IR (2% KBr pellet, 2000–400 cm^{-1}):1634(m), 1589(vs), 1569(w), 1464(m), 1396(w), 1375(w), 1280(m), 1080(s), 1014(s), 947(vs), 910(s, br), 820(vs), 750(w), 721(m), 514(sh).

1.2 Preparation of the PEO–POM electrolyte

The PEO–POM composite polymer electrolyte membrane was prepared by a traditional solution casting method. The POM crystals were harvested and dried under

180 ℃ to remove solvent water molecules. Then, the sample was ground and added into the acetonitrile (Acros, 99.9%) at the ratio of 30% (*w*/*w*) of the total electrolyte. PEO (M_n = 600,000) and bistrifluoromethanesulfonimide lithium salt (LiTFSI) at the ratio of 18: 1 were subsequently dissolved into the above solution, ultrasonically dispersed, stirred at room temperature for 12 h. After that, the mixture was poured into the petri dishes, evaporated the solvent and filled with a mold with the diameter is 16 mm for obtaining the PEO–POM electrolyte membranes. The procedure for PEO–PW_9 electrolyte membrane was prepared as the method with {PW_9} power substituted of POM crystals. And the PEO electrolyte membrane was prepared without the addition of POM crystals. All experiments were operated in glove boxes with argon gas.

(2) Instruments and Physical Measurements

Fourier transform infrared (FTIR) spectra (KBr pellets) were obtained on a FTIR spectrophotometer (Nicolet Avatar 360, Thermo Scientific). Elemental analyses were performed on elemental analyzer (Vario EL III analyzer, Elementar) and inductively coupled plasma-optical emission spectroscopy (ICP-OES, PerkinElmer 8300). Power X-ray diffraction (PXRD) was measured on a PANalytical X' Pert PRO instrument with Cu Kα radiation (λ = 1.54056 Å) in the angular (2θ) range from 5 to 60° at 293K. XPS data were obtained from X-ray photoelectron spectroscopy (XPS, Thermo K-Alpha). Thermal gravimetric curves were conducted with Thermogravimetric Analysis (TG, SDT-Q600) under N_2 flow with 10 °C/min heating. Differential scanning calorimetry (DSC) measurements were conducted on a TA Instrument (DSC3) with a heating rate

of 20 ℃ min^{-1} from –80 to 200 ℃ under a flowing N_2 atmosphere. The microstructure of electrolytes, interface contact and elemental distribution of POM cluster in PEO matrix were observed on scanning electron microscope (SEM, ZEISS Gemini 300) coupled with energy dispersive spectroscopy (EDS, OXFORD XPLORE30). The surface mechanical performance of the electrolytes was performed by in-situ nanoindentation instrument (Hysitron TI 980 TriboIndenter) with a constant pressure of 1000 μN. The tensile strength and elastic modulus of electrolytes were obtained by using tensile tester (AG-X plus) with a 1000 N sensor at a speed of 50mm/min^{-1}. The samples were prepared for tensile testing in a rectangular piece with dimensions of 10 mm × 30 mm (width × length).

Single-crystal X-ray diffraction: suitable crystals were coated with Paratone N oil, suspended on a small fiber loop, and placed in a cooled nitrogen stream at 173(2) K on a Bruker D8 Quest X-ray diffractometer equipped with an Incoatec Microfocus Ga Source (IμS 3.0) and a PHOTON II CPAD detector. A sphere of data was measured using a series of combinations of ϕ and ω scans 10s frame exposures and 0.5° frame widths. Data collection, indexing, frame integration, and final cell refinements were all handled using APEX III software. The SADABS program was used to carry out absorption corrections. The structure was solved using Direct Methods and difference Fourier techniques (SHELXTL, V6.14).

(3) Electrochemical Measurements

The polymer electrolyte films with a thickness of 0.10 to 0.15 mm was sandwiched between two stainless steel sheets for electrochemistry measurements. The electrochemical impedance spectroscopy was measured using an electrochemical working station (CHI660E) with a voltage amplitude of 5 mV over a frequency range from 0.1 to 1000000 Hz.

The ionic conductivity was calculated using the following equation:

$$\sigma = \frac{l}{SR}$$

Where l represents thickness (cm) the of electrolyte, R the resistance of battery and S the contact area (cm^2) between steel sheet and electrolyte.[2] The lithium-ion transference number (t_{Li+}) was calculated based on the equation:

$$t_{Li+} = \frac{I_s}{I_0}\frac{\Delta V - I_0 R_0}{\Delta V - I_S R_S}$$

Where I_0 represents the initial current, I_s is the steady current, and ΔV refers to the direct current polarization voltage of 0.12 V applied to the Li/SPE/Li cells with PEO–POM or PEO electrolytes. R_0 is the initial resistance and R_s is the final steady-state resistance, which were obtained before and after the DC polarization measurement.[3] Electrochemical stability of the electrolytes was evaluated by employing linear sweep voltammetry (LSV) with prepared SS/PEO–POM/Li and SS/PEO/Li batteries, and the sweep rate is 1 mV s^{-1}. The galvanostatic charge-discharge behavior of symmetrical cells with the two electrolytes was detected on the battery testing system (BTS-2004, Neware) at 25 °C within the voltage range of 2.5–4.0 V (*vs*. Li^+/Li). Long cycling performance of the PEO–POM electrolyte was evaluated on a $LiFePO_4$/SPE/Li full

battery, and the cathode electrode with a loading of 5 mg·cm^{-2} was equipped by mixing $LiFePO_4$, carbon nanotube (CNT) and poly(vinylidene fluoride) (PVDF) at a weight ratio of 8: 1: 1 in NMPN-methyl-2-pyrroldone (NMP). The first two circles were activated at a low current of 0.1 C and the capacity retention was calculated based on the capacity of the third cycle. All assemblies were carried out in an argon filled glove box.

(4) TGA characterization of 1

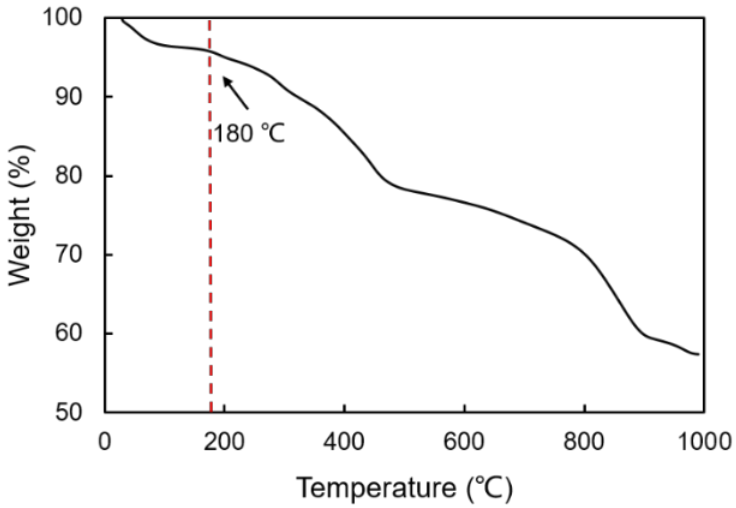

Fig. S1. Thermogravimetric analysis trace of **1**.

The thermal curve of **1** was shown in Figure S1, which was carried out under N_2 atmosphere in the temperature range from 30 ℃ to 1000 ℃. The first loss stage starts from room temperature to 180 ℃, corresponding to the removal of 7 lattice water molecules: (3.99% calculated vs. 3.97%). The second weight loss between 180~500 ℃ was attributed to the loss of three DMA^+ cations and the three PDC ligands: (20.15% calculated vs. 17.63%).

(5) Preparation of PEO–POM membrane and SEM images

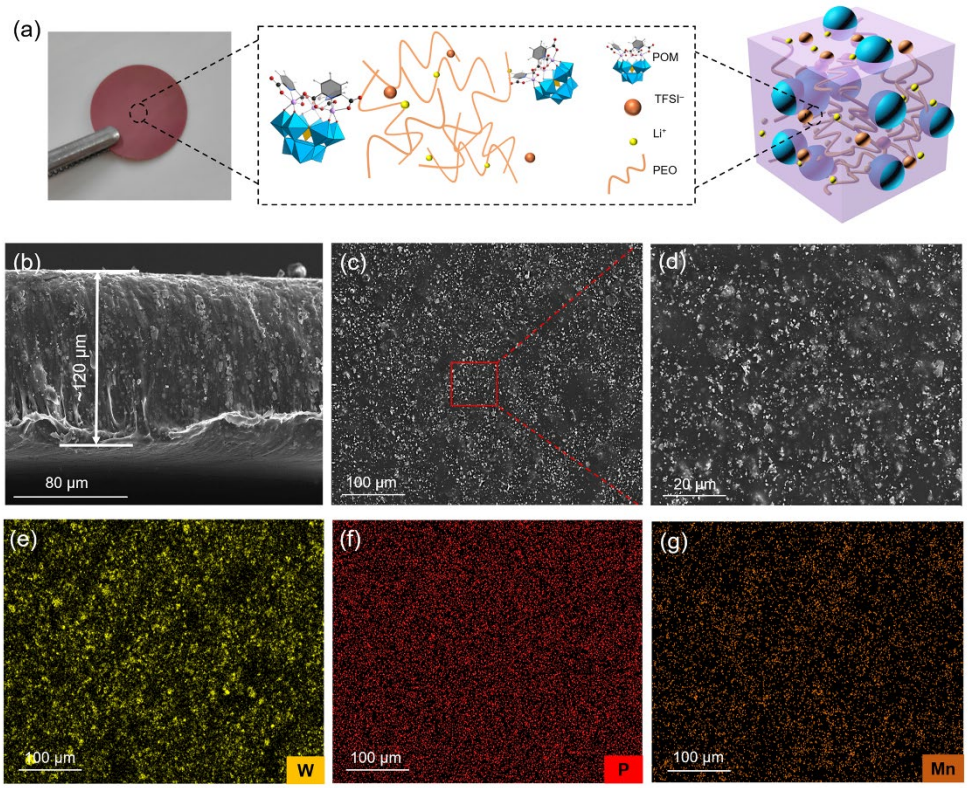

Fig. S2. a) Illustration of the composition of the PEO–POM membrane; b) Cross sectional-view SEM images of the PEO–POM electrolyte membrane; c) Plane-view SEM images of PEO–POM electrolyte membrane; d) The magnified images of marked area in (c); (e-g) Elemental mapping images of the PEO–POM electrolyte membrane. W, yellow; P, red; Mn, orange.

(6) Ionic conductivity of the PEO–{PW_9} electrolyte

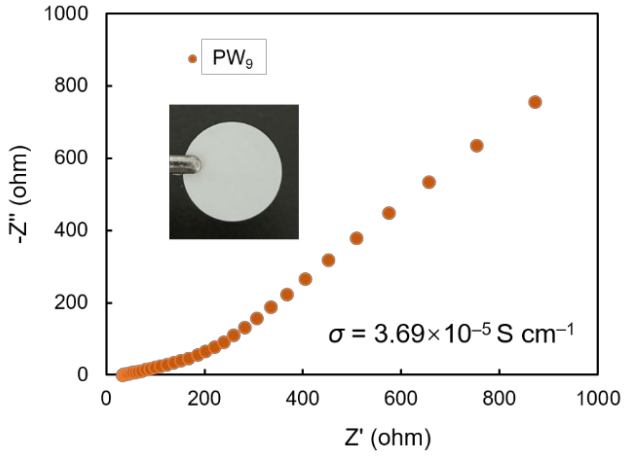

Fig. S3. Electrochemical impedance spectroscopy of the PEO–{PW_9} electrolyte at RT; insert, the photo of the PEO–{PW_9} electrolyte film.

(7) The lithium transference number

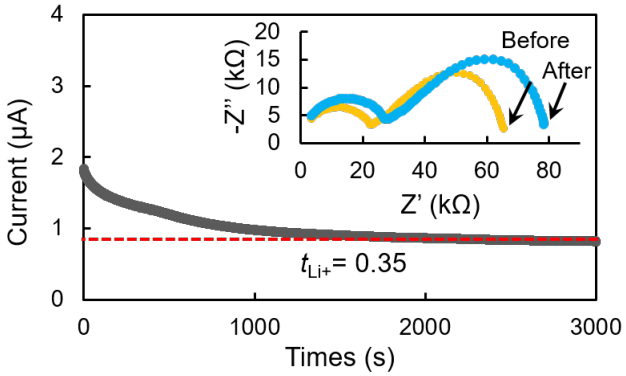

Fig. S4. Chronoamperometry-time curves during the polarization of Li/PEO/Li cell at 25 ℃, followed an applied potential of 0.12 V; Insert: corresponding Nyquist spectra before and after polarization.

(8) In situ SEM measurement, F1s XPS spectra and Nyquist plots

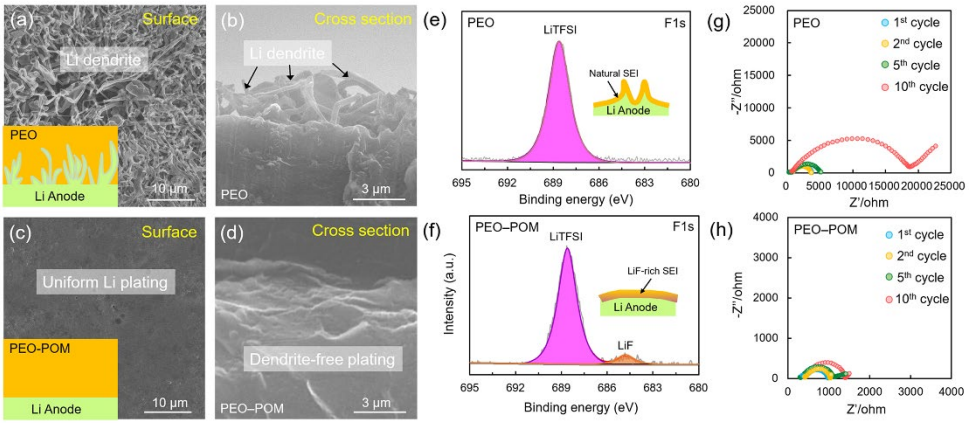

Fig. S5. a) Surface and b) cross-sectional SEM images of the PEO electrolyte after cycling; c) Surface and d) cross-sectional SEM images of PEO–POM composite electrolyte after cycling; The F1s XPS spectra of e) the PEO electrolyte and f) the composite electrolyte; The Nyquist plots of the g) PEO electrolyte and h) PEO–POM composite electrolyte.

(9) The mechanical property measurement of electrolytes

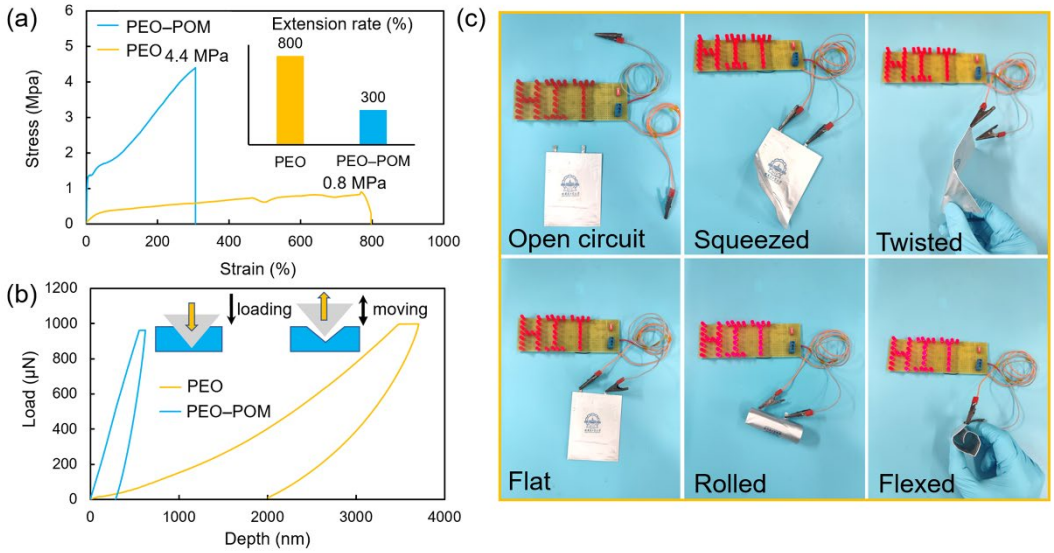

Fig. S6. a) Stress-stain curves of the PEO and PEO–POM electrolytes; b) In-situ nanoindentation curves of the two electrolytes; c) Illustration of the pouch cell powering the LEDs at various physical states.

(10) NMR characterization of 1

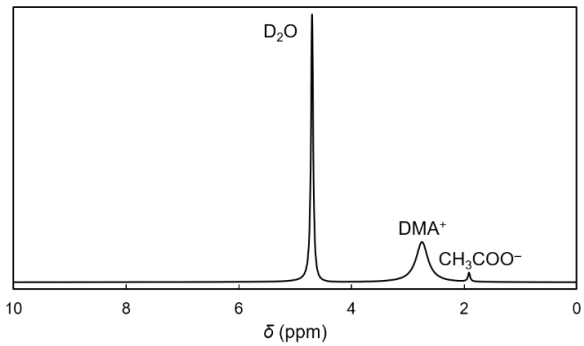

Fig. S7. ^{1}H NMR spectrum of **1**

Due to the paragmagnetic effect of the Mn^{III} centers in **1**, ^{1}H signals of the PDC ligands are too broadened to be observed. The two resonances at 2.7 and 1.9 ppm are from the DMA^{+} counter cations and the methyl protons of acetate impurity, respectively.

(11) Assembly of the button cell battery

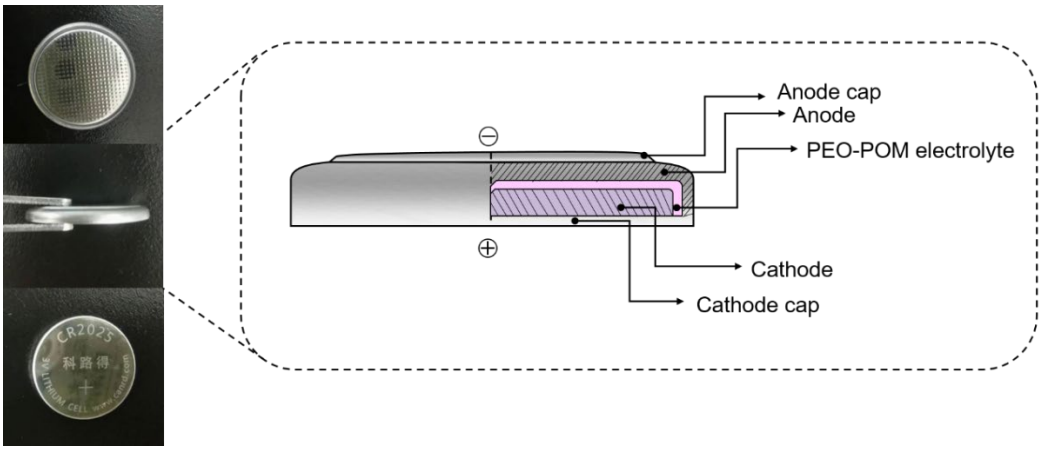

Fig. S8. The assembled button cell battery and a schematic diagram of its inner structure

(11) Single-Crystal X-ray Structure Determination

CCDC 2327293 contain the supplementary crystal data for this paper. These data can be obtained free of charge from The Cambridge Crystallographic Data Centre via www.ccdc. cam.ac.uk/data_request/cif.

Table S1. Crystal data and structure refinement for **1** (CCDC deposit number: 2327293).

Identification code	Monomer	
Empirical formula	$C_{27}H_{50}Mn_3N_6O_{53}PW_9$	
Formula weight	3154.14	
Temperature	193(2) K	
Wavelength	1.34139 Å	
Crystal system	Trigonal	
Space group	*P* 31c	
Unit cell dimensions	a = 18.9481(5) Å	α = 90 °.
	b = 18.9481(5) Å	β = 90 °.
	c = 29.4882(12) Å	γ = 120 °.
Volume	9168.7(6) Å^3	
Z	4	
Density (calculated)	2.285 Mg/m^3	
Absorption coefficient	16.727 mm^{-1}	
F(000)	5724	
Crystal size	0.560 x 0.200 x 0.200 mm^3	
Theta range for data collection	2.342 to 60.354 °.	
Index ranges	$-23 \leqq h \leqq 24$, $-23 \leqq k \leqq 24$, $-33 \leqq l \leqq 37$	
Reflections collected	60704	
Independent reflections	11811 [R(int) = 0.0430]	
Completeness to theta = 23.337 °	99.8 %	
Absorption correction	Semi-empirical from equivalents	
Refinement method	Full-matrix least-squares on F^2	
Data / restraints / parameters	11811 / 13 / 559	
Goodness–of–fit on F^2	1.073	
Final R indices [I>2sigma(I)]	R_1 = 0.0381, ωR_2 = 0.1083	
R indices (all data)	R_1 = 0.0427, ωR_2 = 0.1111	
Largest diff. peak and hole	1.348 and -1.324 e.Å^{-3}	

(12) BVS calculation

For determination of the oxidation states of Mn centers and the protonation states of oxygen sites, BVS calculations were carried out using the method of I. D. Brown.[4] The r_o values were taken from the literature.[5] for calculations performed on Mn**.**

Table S2. BVS calculations for Mn sites in compound **1**

Compounds	Manganese atoms	BVS			Assigned oxidation states
		Mn(II)	Mn(III)	Mn(IV)	
1	Mn1	3.146	**2.989**	3.078	III
	Mn2	3.202	**2.977**	3.097	III

(13) DSC measurements

Table S3. T_g, T_m, ΔH_m, and χ_c of PEO and PEO–POM electrolytes

	T_g (°C)	T_m (°C)	ΔH_m (J g^{-1})	Crystallinity (χ_c)
PEO	−39.88	57.60	32.77	15.33%
PEO–POM	−46.05	56.66	25.33	11.85%

(for the degree of crystallinity the same heat of fusion was employed for the 100% crystalline PEO, namely 213.7 J g^{-1}).[6]

References

S1 A.P. Ginsberg, Inorganic Syntheses, John Wiley & Sons, Inc, 1990, pp. 100.

S2 Z. Lu, L. Peng, Y. Rong, E. Wang, R. Shi, H. Yang, Y. Xu, R. Yang, C. Jin, *Energy Environ. Mater.* (2023).

S3 H. An, Q. Liu, J. An, S. Liang, X. Wang, Z. Xu, Y. Tong, H. Huo, N. Sun, Y. Wang, Y. Shi, J. Wang, *Energy Stor. Mater.,* 2021, **43**, 358-364.

S4 I. D. Brown and D. Altermatt, *Acta. Cryst*., 1985, **41**, 244-247.

S5 N. E. Brese and M. Okeeffe, *Acta. Crystallogr. B*, 1991, **47**, 192–197.

S6 X. Wu, K. Chen, Z. Yao, J. Hu, M. Huang, J. Meng, S. Ma, T. Wu, Y. Cui and C. Li, *J. Power Sources*, 2021, **501**, 229946.